Originally published as:

Göttl, F., and R. Rummel (2009), A geodetic view on isostatic models, Pure and Applied Geophysics, 166(8-9), 1247–1260

DOI: 10.1007/s00024-004-0489-x

Note: This is the accepted manuscript and may marginally differ from the published version.

A Geodetic View on Isostatic Models

Franziska Göttl,[1] and Reiner Rummel [2]

[1]Deutsches Geodätisches Forschungsinstitut, München, Germany

[2]Institut für Astronomische und Physikalische Geodäsie, Technische Universität München, Germany

Contact:

F. Göttl, Deutsches Geodätisches Forschungsinstitut, Alfons-Goppel-Str. 11, 80539 München, Germany. (goettl@dgfi.badw.de; Tel: 0049-(0)89-230311119)

R. Rummel, Institut für Astronomische und Physikalische Geodäsie, Arcisstr. 21, 80333 München, Germany. (rummel@bv.tu-muenchen.de; Tel: 0049-(0)89-28923190)

Abstract – Before the background of more accurate and denser gravity data it is worthwhile to reassess geodetic isostasy. Nowadays, in geodesy isostatic models are primarily applied to gravity reduction as needed by geoid and gravity modeling. The selection of the isostatic model is based on four criteria: Isostatically reduced gravity anomalies should be (1) geophysically meaningful, (2) easy to compute, (3) small, smooth and therefore easy to interpolate and (4) the indirect effect, i. e. the change of potential and gravity due to isostatic mass replacement, should be small. In this study we analyze free air anomalies as well as isostatic anomalies based on the Airy-Heiskanen model and on the Pratt-Hayford model in regard to these criteria. Several facts suggest that free air anomalies are the most realistic type of isostatic anomalies. They reflect the actual isostatic compensation, are easy to compute and their indirect effect is negligibly small. However, they are not smooth due to the fact that local topographic loads are only partially compensated. Smoothness can be achieved by introducing either a mathematical low-pass filter or a hydrostatic isostatic model, such as the Airy-Heiskanen or the Pratt-Hayford model. In both cases the resulting isostatically reduced gravity anomalies fulfill all requirements. In order to improve the numerical efficiency, a new mathematical description of the Pratt-Hayford model is formulated. The level of smoothing with respect to free air anomalies is analyzed in global and regional contexts. It turns out that the mechanism of mass compensation in regions of large topographic loads is better described by the Airy-Heiskanen model, whereas the Pratt-Hayford model is more suitable for regions of deep ocean trenches.

Key words: Airy-Heiskanen model, free air gravity anomalies, isostatic gravity anomalies, Pratt-Hayford model

1 Introduction

Isostasy describes the phenomenon of compensation of topographic loads. Gravity anomalies and deflections of the vertical, as derived from topographic masses, are much larger than the corresponding values based on measurements. More than 250 years ago this led to the hypothesis of isostatic mass compensation, which was confirmed about 100 years later by field measurements (Heiskanen, 1950). Investigations of this theory belong to the interdisciplinary field of geodynamics, because they combine geodetic, geophysical and geological observations and knowledge. A comprehensive treatise on the development of isostasy and its state-of-the art is the monograph by Watts (2001). In geophysics the concepts of isostasy are used to explain the mechanism of mass compensation

and that of the flexure of the lithosphere under topographic loading. Isostasy is also the mechanism underlying glacial isostatic adjustment, see e.g. Wolf (1993). It is also a key to an improved understanding of planetary evolution (Schubert *et al.*, 2001; Watts, 2001). In geodesy isostatic models are primarily applied to gravity reduction in the context of the solution of the Geodetic Boundary Value Problem (GBVP), i. e. the determination of the gravity field at the Earth's surface and in its exterior as well as the determination of the geoid. The aim is to obtain smooth and representative data, which can be easily interpolated. The selection of the isostatic model is thereby based on four criteria: Isostatically reduced gravity anomalies should be (1) geophysically meaningful, (2) easy to compute, (3) small, smooth and therefore easy to interpolate and (4) the indirect effect, i. e. the change of potential and gravity due to isostatic mass replacement, should be small. These four characteristics were discussed in the classical geodetic monograph by Heiskanen and Moritz (1967). The fact that gravity data are getting more accurate and denser and numerical computations more efficient makes it worthwhile to revisit "geodetic isostasy" with these four criteria in mind. Recent studies along this line are Rummel *et al.* (1988); Engels *et al.* (1995); Kaban *et al.* (1999); Tsoulis (2001, 2004); Claessens (2003); Kuhn (2003); Heck and Wild (2005); Wild and Heck (2005) as well as Wild-Pfeiffer (2007).

2 Isostatic models

The basic understanding is that the load of topographic masses requires some mechanism of support or compensation. The two models commonly employed in geodesy are the Airy-Heiskanen and the Pratt-Hayford model. They will be discussed below. As mentioned in Turcotte and Schubert (1982) or in Watts (2001) a variety of actual geodynamic processes may be approximated by them. The weakness of both models is that they assume local compensation: the topographic load is compensated column-wise; hence the elastic flexural rigidity of the lithospheric plate is ignored. An advantage is that simple mathematical models of isostasy can be formulated. For instance, the Vening-Meinesz model of regional isostasy tries to avoid local compensation (e.g. Wolf, 1984; Moritz, 1990; Watts, 2001). Furthermore, it is known that only larger mountains are compensated, while local topographic features with an extension of less than 100 km are supported by the lithosphere underneath (Torge, 2003).

A gravimeter measures the gravitational attraction of the mass distribution. This implies that

free air anomalies, whether computed at the geoid (Stokes) or the terrain (Molodenskii), are the most realistic type of isostatic anomalies. This is the reason why free air anomalies are small and produce only a small indirect effect. However, they are not very smooth due to the local topographic features which are not locally compensated. Except for the lack of smoothness all of the above-mentioned criteria are fulfilled. Smoothness can be attained by low-pass filtering of the free air anomalies.

If the contribution of the topographic masses is subtracted from the measurements, Bouguer gravity anomalies are obtained. They are smooth but rather large and anti-correlated with the large topography features due to the neglect of mass compensation. Thus, interpolation is easy but the actual mass distribution is modified significantly, resulting in a large indirect effect (criteria 4).

A logical step is therefore to introduce a model of isostatic compensation. The **Airy-Heiskanen model** assumes the lighter crust ($\rho_{cr} = 2.67$ g cm^{-3}) to float on the denser mantle ($\rho_m = 3.27$ g cm^{-3}). The displaced mantle volume produces buoyancy, which results in a state of equilibrium. Mass surpluses of topography are compensated by what is known as roots of the low-density crust whereas mass deficiencies of the oceans are compensated by anti-roots of the higher-density mantle. The boundary between the Earth's crust and mantle corresponds to the Mohorovičić-discontinuity of seismology. Usually an average crustal thickness of $T = 30$ km is adopted. Other values of average crustal thickness were tested as well, see e.g. Heiskanen (1950). A schematic view of the Airy-Heiskanen model is displayed in Fig. 1. Crustal thickening underneath the Himalayas, Andes and Alps suggest this model to apply. On the other hand, for deep ocean trenches the assumptions of the Airy-Heiskanen model leads to unrealistical or even negative crustal thickness, see Claessens (2003). As an alternative the **Pratt-Hayford model** may be used. It assumes equal weight of each independent lithospheric mass column. Thus, hydrostatic equilibrium holds at a constant depth of compensation D. Mass surpluses and deficiencies are compensated by a variable density ρ_i of each column of the lithosphere. The reference or standard column is defined by a depth D corresponding to an average thickness of the lithosphere of 100 km and by a density ρ_0 corresponding to an average lithospheric density of 2.915 g cm^{-3}. For other assumptions, see Heiskanen (1950). The model is shown in Fig. 2. With both the Airy-Heiskanen and the Pratt-Hayford models all but the first criterion are largely met. Most of the above has already been discussed in the literature, see e.g. Heiskanen and Moritz (1967) and Rummel *et al.* (1988). Kaban *et al.* (2004) showed that realistical conclusions about the actual isostatic state of the lithosphere require detailed

local studies and the use of data representative of the crustal structure and density distribution.

3 Computation of isostatically reduced gravity anomalies

As early as in the fifties and sixties it was concluded that the use of isostatic modeling was important to obtain an accurate solution of the GBVP. However, numerical challenges were still great at that time. This led to the development of efficient numerical models of isostasy, see e.g. Heiskanen and Moritz (1967). Nowadays, it is mainly the vast amount of topographic data that requires efficient algorithms. In the following, the numerical implementation of isostatic models will be discussed.

Free air gravity anomalies are very simple to calculate. The basic formula is

$$\Delta g^{FAR} = g + FAR_1 + FAR_2 - \gamma \tag{1}$$

with g the measured gravity at some surface point, FAR_1 and FAR_2 the linear and quadratic free air correction (Gruber, 2000) and γ the normal gravity at the corresponding foot point on the reference ellipsoid. In geodesy an internationally adopted normal gravity field without geophysical significance is employed for γ, while in geophysics an equilibrium figure is sometimes used (Nakiboglu, 1982). The above formula holds for the Stokes and the Molodenskii type solution of the GBVP, although with a different interpretation.

The computation of **isostatic gravity anomalies of type Airy-Heiskanen** is more complicated. To improve numerical efficiency, first of all the difference in treatment of ocean and land areas in the Airy-Heiskanen column model displayed of Fig. 1 must be converted into a uniform column model (e.g. Rummel *et al.*, 1988).

Approximate position of Fig. 1!

For this purpose the mass deficiency of the oceans due to the lower density of water ($\rho_{ocean} = 1.03$ g cm^{-3}) is replaced by an equivalent layer with crustal density. The resulting ocean depths are denoted by "equivalent-rock" topography h. They can be obtained by the following equation which takes into account the convergence of the columns (Mladek, 2006):

$$h = -R + \left(\frac{\rho_{ocean} R^3 + (\rho_{cr} - \rho_{ocean})(R - H_W)^3}{\rho_{cr}} \right)^{\frac{1}{3}}, \tag{2}$$

where $R = 6378137$ m is the reference Earth radius and H_W is the water depth. Now the condition of mass equilibrium $\int_{r=R}^{R+h} \rho_{cr} r^2 dr = \int_{r=R-T-t}^{R-T} (\rho_m - \rho_{cr}) r^2 dr$ can be applied equally for land and

ocean columns. $T = 30$ km denotes the compensation depth and t the (anti-)root thickness. A further benefit of this approach is that only one formula is needed for calculating the root as well as the anti-root thickness:

$$t = \frac{\rho_{cr}}{\rho_m - \rho_{cr}} \left(\frac{R}{R-T} \right)^2 h. \tag{3}$$

RUMMEL *et al.* (1988) showed that the error of linear approximation remains below 1 %. After introducing the uniform Airy-Heiskanen column model isostatic gravity anomalies can be determined in four steps. In the following, all isostatic computations will be implemented in terms of global spherical harmonic analysis and synthesis. Thereby, in order to avoid integration in the radial direction, "equivalent-rock" topographic heights are expanded into a Taylor series up to the third power. The spherical harmonic coefficients of topographic heights are kept dimensionless by dividing them by the Earth's radius. For more details see RUMMEL *et al.* (1988) or TSOULIS (1999). The resulting set of normalized dimensionless potential coefficients $\overline{C}^T_{nm}$ and $\overline{S}^T_{nm}$ of topography is

$$\left.\begin{matrix} \overline{C}^T_{nm} \\ \overline{S}^T_{nm} \end{matrix}\right\} = \frac{3}{2n+1} \cdot \frac{\rho_{cr}}{\overline{\rho}_{earth}} \left[\left\{ \begin{matrix} \overline{h}_{nmc} \\ \overline{h}_{nms} \end{matrix} \right\} + \frac{(n+2)}{2} \left\{ \begin{matrix} \overline{h2}_{nmc} \\ \overline{h2}_{nms} \end{matrix} \right\} + \frac{(n+2)(n+1)}{6} \left\{ \begin{matrix} \overline{h3}_{nmc} \\ \overline{h3}_{nms} \end{matrix} \right\} \right] \tag{4}$$

with the mean Earth density $\overline{\rho}_{earth} = 5.52$ g cm^{-3} and the linear, quadratic and cubic topographic cosine (c) and sine (s) coefficients $\overline{h}_{nm}$, $\overline{h2}_{nm}$, $\overline{h3}_{nm}$ of degree n and order m following from a series expansion of the dimensionless linear, squared and cubic height functions h/R. From this set of coefficients, the refined Bouguer Topographic Reduction (BTR) is computed by

$$\left.\begin{matrix} \overline{A}^T_m(\theta) \\ \overline{B}^T_m(\theta) \end{matrix}\right\} = \sum_{n=m}^{N} \overline{P}_{nm}(\cos\theta) \left\{ \begin{matrix} -\frac{GM}{R^2}(n+1)\overline{C}^T_{nm} \\ -\frac{GM}{R^2}(n+1)\overline{S}^T_{nm} \end{matrix} \right. \tag{5}$$

$$\text{and} \quad BTR(\theta,\lambda) = \sum_{m=0}^{N} \overline{A}^T_m(\theta)\cos m\lambda + \overline{B}^T_m(\theta)\sin m\lambda, \tag{6}$$

where λ is the longitude and θ the colatitude of the integration point, GM is the product of the gravitational constant and the mass of the Earth and $\overline{P}_{nm}(\cos\theta)$ are the fully normalized associated Legendre polynomials. By adding this reduction to the free air anomalies according to Eq. 1 one obtains Bouguer gravity anomalies. As explained before they are smooth, but highly anti-correlated with terrain. They refer to an Earth without topography (geoid) but with mass compensation embedded in the lithosphere. In case of the Airy-Heiskanen isostatic model of root thickness t and

average crustal thickness T, the coefficients of mass compensation are

$$\left.\begin{matrix}\overline{C}^C_{nm}\\ \overline{S}^C_{nm}\end{matrix}\right\} = -\frac{3}{2n+1}\cdot\frac{\rho_{cr}}{\overline{\rho}_{earth}}\left[\left(\frac{R-T}{R}\right)^n\left\{\begin{matrix}\overline{h}_{nmc}\\ \overline{h}_{nms}\end{matrix}\right\} - \frac{(n+2)}{2}\frac{\rho_{cr}}{\rho_m-\rho_{cr}}\left(\frac{R-T}{R}\right)^{n-3}\left\{\begin{matrix}\overline{h2}_{nmc}\\ \overline{h2}_{nms}\end{matrix}\right\}\right.$$
$$\left. +\frac{(n+2)(n+1)}{6}\left(\frac{\rho_{cr}}{\rho_m-\rho_{cr}}\right)^2\left(\frac{R-T}{R}\right)^{n-6}\left\{\begin{matrix}\overline{h3}_{nmc}\\ \overline{h3}_{nms}\end{matrix}\right\}\right]. \quad (7)$$

From this set of coefficients the Airy Heiskanen Correction (AHC) is obtained via

$$\left.\begin{matrix}\overline{A}^C_m(\theta)\\ \overline{B}^C_m(\theta)\end{matrix}\right\} = \sum_{n=m}^{N}\overline{P}_{nm}(\cos\theta)\left\{\begin{matrix}-\frac{GM}{R^2}(n+1)\overline{C}^C_{nm}\\ -\frac{GM}{R^2}(n+1)\overline{S}^C_{nm}\end{matrix}\right. \quad (8)$$

$$\text{and}\quad AHC(\theta,\lambda) = \sum_{m=0}^{N}\overline{A}^C_m(\theta)\cos m\lambda + \overline{B}^C_m(\theta)\sin m\lambda. \quad (9)$$

The resulting isostatic gravity anomalies are computed via

$$\Delta g^{Airy} = g + FAR_1 + FAR_2 - \gamma + BTR + AHC + \delta g. \quad (10)$$

The indirect effect due to the replacement of topography and topographic roots is small and given by

$$\delta g = \frac{2}{R}(V^T + V^C) \quad (11)$$

in terms of gravity perturbation. Here V^T is the gravity potential derived from the topography and V^C that from the compensating masses. It is sometimes claimed that in the case of perfect isostatic compensation the resulting gravitational attraction would be zero. The comparison of Eq. 4 with Eq. 7 shows, however, that even in linear approximation this is only true if $T = 0$ km. In the actual case the crustal layer of thickness $T = 30$ km acts as a filter damping the gravity contributions of the balancing masses at depth. For increasing T the effect of compensation is getting smaller and becomes zero for $T = R$.

Recently, an efficient method for the determination of **isostatic gravity anomalies of type Pratt-Hayford** has been established. This approach is shown in Fig. 3 and explained in Mladek (2006).

Approximate position of Fig. 2 and Fig. 3!

The condition of equilibrium of mass for each column is

$$\int_{r=R-D}^{R-h}\rho_i r^2 dr = \int_{r=R-D}^{R}\rho_0 r^2 dr. \quad (12)$$

Here, D is the depth of compensation and ρ_0 is the average density of the lithosphere. For ocean areas the Pratt-Hayford model contains two unknowns: the "equivalent-rock" topographic height h

and the density ρ_i. Solving for the column density yields

$$\rho_i = \rho_0 \left(\frac{R^3 - (R-D)^3}{(R-h)^3 - (R-D)^3} \right). \tag{13}$$

In order to be able to treat ocean columns like land columns, the water part of the ocean column with depth H_W must be replaced by equivalent rock of height $H_W - h$ and density ρ_i, see Fig.3. This leads to the condition $\int_{r=R-H_W}^{R} \rho_{ocean} r^2 dr = \int_{r=R-H_W}^{R-h} \rho_i r^2 dr$. By inserting Eq. 13 the solution for h is found to be

$$h = \left(\frac{k}{l} \right)^{\frac{1}{3}} - R \quad \text{with} \quad l = \rho_{ocean} \left[R^3 - (R-H_W)^3 \right] - \rho_0 \left[R^3 - (R-D)^3 \right] \tag{14}$$

$$\text{and} \quad k = \rho_0 (R-H_W)^3 \left[-R^3 + (R-D)^3 \right] - \rho_{ocean} (R-D)^3 \left[-R^3 + (R-H_W)^3 \right]. \tag{15}$$

The remaining computations are straightforward. The normalized, dimensionless potential coefficients of the lithospheric columns of length $D+h$ and density ρ_i are obtained by

$$\begin{aligned} \left. \begin{matrix} \overline{C}_{nm} \\ \overline{S}_{nm} \end{matrix} \right\} &= \frac{3}{2n+1} \cdot \frac{\rho_0}{\overline{\rho}_{earth}} \left[\left\{ \begin{matrix} \overline{h}_{nmc} \\ \overline{h}_{nms} \end{matrix} \right\} + \frac{(n+2)}{2} \left\{ \begin{matrix} \overline{h2}_{nmc} \\ \overline{h2}_{nms} \end{matrix} \right\} + \frac{(n+2)(n+1)}{6} \left\{ \begin{matrix} \overline{h3}_{nmc} \\ \overline{h3}_{nms} \end{matrix} \right\} \right] \\ &\quad + \frac{3}{(2n+1)(n+3)} \cdot \frac{\rho_0}{\overline{\rho}_{earth}} \left[1 - \left(\frac{R-D}{R} \right)^{n+3} \right] \left\{ \begin{matrix} \overline{\rho}_{nmc} \\ \overline{\rho}_{nms} \end{matrix} \right\}. \end{aligned} \tag{16}$$

Here, the linear, quadratic and cubic topographic coefficients $\overline{h}_{nm}$, $\overline{h2}_{nm}$, $\overline{h3}_{nm}$ follow from a series expansion of the dimensionless linear, squared and cubic height functions h/R times the dimensionless density function ρ_i/ρ_0. The density function is obtained from Eq. 13. The coefficients $\overline{\rho}_{nmc}$ and $\overline{\rho}_{nms}$ are derived from a direct spherical harmonic expansion of ρ_i/ρ_0, for details see Mladek (2006). With the coefficient set $\overline{C}_{nm}$ and $\overline{S}_{nm}$ the lithospheric columns are removed. This procedure is therefore called remove step (REM):

$$\left. \begin{matrix} \overline{A}_m(\theta) \\ \overline{B}_m(\theta) \end{matrix} \right\} = \sum_{n=m}^{N} \overline{P}_{nm}(\cos\theta) \left\{ \begin{matrix} -\frac{GM}{R^2}(n+1)\overline{C}_{nm} \\ -\frac{GM}{R^2}(n+1)\overline{S}_{nm} \end{matrix} \right. \tag{17}$$

$$\text{and} \quad REM(\theta,\lambda) = \sum_{m=0}^{N} \overline{A}_m(\theta)\cos m\lambda + \overline{B}_m(\theta)\sin m\lambda. \tag{18}$$

Afterwards, a homogeneous and spherical lithospheric shell is restored, represented by only one spherical harmonic coefficient:

$$\overline{C}_{n=0,m=0} = -\frac{\rho_0}{\overline{\rho}_{earth}} \frac{R^3 - (R-D)^3}{R^3}, \tag{19}$$

which leads to the gravitational potential of a spherical shell. This is called the restore step (RES):

$$RES(\theta,\lambda) = -\frac{GM}{R^2} \overline{C}_{n=0,m=0}. \tag{20}$$

One ends up with isostatic gravity anomalies of type Pratt-Hayford:

$$\Delta g^{Pratt} = g + FAR_1 + FAR_2 - \gamma + REM + RES + \delta g. \tag{21}$$

They refer to an Earth without topography and with a spherical and homogenous lithosphere of 100 km thickness. The indirect effect resulting from this change of mass distribution is small. It is

$$\delta g = \frac{2}{R}(V^{REM} + V^{RES}) \tag{22}$$

in terms of a gravity perturbation. Here, V^{REM} is the gravity potential derived from the heterogeneous lithosphere and V^{RES} that from the homogenous lithosphere of constant thickness.

4 Signal size and smoothness of isostatic gravity anomalies

In the previous section it has been shown that efficient numerical algorithms can be constructed for the isostatic models of Airy-Heiskanen and Pratt-Hayford. In this section the signal characteristics and the level of smoothness of free air, Airy-Heiskanen and Pratt-Hayford gravity anomalies are discussed.

Figures 4 show these three types of gravity anomaly based on the Earth Gravity Model 1996 (EGM96) up to degree and order 360 and the elevation model JPG95E. Free air anomalies exhibit higher variability, especially in mountain and ocean trench areas, than do Airy-Heiskanen or Pratt-Hayford isostatic anomalies. This is also verified by the root mean square values (RMS), which amount to 27 mGal for Δg^{FAR}, 22 mGal for Δg^{Airy} and 24 mGal for Δg^{Pratt}. If a Gaussian filter with a smoothing radius of 50 km is applied to the free air anomalies, their RMS is reduced to 22 mGal. This shows that smoothed free air anomalies do not show higher variability than Airy-Heiskanen or Pratt-Hayford isostatic anomalies. Further, it can be concluded that the free air anomalies are higher correlated with local topography, whereas isostatic anomalies are quite independent of topography.

Approximate position of Fig. 4!

This can also be seen in the differences of free air anomalies and isostatic anomalies of type Airy-Heiskanen and Pratt-Hayford respectively (Fig. 5), which display topographic patterns, such as mountains and ocean ridges. Even though free air anomalies are isostatic anomalies too, these differences are rather large; the RMS differences amount to 16 mGal for the isostatic approach of Airy-Heiskanen and 26 mGal for the Pratt-Hayford model. Reasons could be that, neither of the

two models is conforming to reality.

Approximate position of Fig. 5!

The level of smoothness of the three types of gravity anomaly can be checked by their corresponding degree variances $c_n^2(\Delta g^{FAR})$, $c_n^2(\Delta g^{Airy})$ and $c_n^2(\Delta g^{Pratt})$ (Fig. 6). Degree variances represent the spectral power of global signals. One can see that isostatic anomalies of type Airy-Heiskanen and Pratt-Hayford are smoother for higher degrees than are free air anomalies. Degree variances of smoothed free air anomalies exhibit a high agreement with degree variances of Pratt-Hayford anomalies up to degree 125.

Approximate position of Fig. 6!

As an indication of the level of smoothing we determine smoothing values per spherical harmonic degree with

$$s_n = 100 - \sqrt{\frac{c_n^2(\Delta g^{Airy/Pratt})}{c_n^2(\Delta g^{FAR})}} \cdot 100. \tag{23}$$

They provide a measure of the percentage of smoothing per degree of the isostatic Airy-Heiskanen/Pratt-Hayford relative to the free air anomalies, see Fig. 7. Up to degree 10 nearly no smoothing occurs. For the range between degree 100 and 200 the two isostatic models show a similar smoothing level of about 25 %. Outside this range the isostatic anomalies based on the Airy-Heiskanen model exhibit 10 % higher smoothing values than the isostatic anomalies based on the Pratt-Hayford model. Beyond degree 200 the level of smoothing decreases.

Approximate position of Fig. 7!

The models by Airy-Heiskanen and by Pratt-Hayford are now tested for typical tectonic settings. The question under investigation is which of these two isostatic models yields smaller residuals when compared to the free air anomalies. We select for our tests the following regions: Alps, Andes, Himalayas, Mariana Trench, Puerto-Rico-Trench and Atacama Trench. The statistics, range of the values, mean and RMS value are shown in Tab. 1. We conclude that smoothing is higher in regions of large topographic variability, such as the Andes and the Himalayas. In these regions a smoothing of around 39 % can be reached for both isostatic models. In the Alps only the Airy-Heiskanen model achieves a smoothing of about 11 %. Thus, the Airy-Heiskanen model is superior for large mountain chains. For deep ocean trenches, such as the Mariana and the Atacama Trenches, the Pratt-Hayford model achieves a smoothing of around 41 %, whereas that of Airy-Heiskanen reaches only 31 %. Therefore, the isostatic assumption of Pratt-Hayford seems to apply for deep ocean trenches. This suggests the use of the Airy-Heiskanen model in continental regions and of the Pratt-Hayford model

in oceanic regions, as recommended by Wild and Heck (2005). In order to optimize the individual model results, one may vary the free parameters of the models: in case of Airy-Heiskanen the compensation depth and in case of Pratt-Hayford the compensation depth and/or the density of the normal column. Helpful suggestions are given in Rummel *et al.* (1988).

Approximate position of Tab. 1!

5 Conclusions

In this study four basic criteria for isostatic modeling in geodetic applications are tested: (1) geophysically significance, (2) simplicity of computation, (3) case of interpolation and (4) smallness of the indirect effect. Free air anomalies directly reflect the state of isostatic compensation. While free air anomalies are relatively small and smooth on large and medium scales, they are rugged and strongly correlated with local, uncompensated topography on short scales. They are easy to compute and their indirect effect is negligibly small. For geoid determination smoothness is an important requirement, because interpolation may be needed in case of regional under-sampling or data gaps. One option to attain smoothness is low-pass filtering of free air anomalies (using e.g. a Gaussian filter with optimized radius). The drawback of this is the loss of physical information. Smoothness can be also achieved by using isostatic models, such as the Airy-Heiskanen or the Pratt-Hayford models. They are based on hypotheses of mechanisms of local isostatic mass compensation. Small isostatic anomalies indicate that the model choice is correct from a geophysical point of view. However, as shown by Kaban *et al.* (2004), realistic conclusions about the actual state of isostatic mass balance require local analysis and the use of complementary crustal and lithospheric data. Thus, we conclude that the models of Airy-Heiskanen and Pratt-Hayford provide only an approximation of the state of isostatic compensation. Both models fulfill, however, the geodetic criteria of simplicity, smoothness and small indirect effect. It can be shown that an efficient numerical computation is possible for the Pratt-Hayford approach, similar to the one widely used for the Airy-Heiskanen model. Numerical studies show that the model of Airy-Heiskanen applies for mass compensation of major mountain ranges, such as Himalayas, Andes and Alps, whereas the model of Pratt-Hayford fits better for deep ocean trenches, such as Mariana, Puerto-Rico or Atacama., see also Claessens (2003). Globally, isostatically reduced free air gravity anomalies based on the Airy-Heiskanen model are about 10 % smoother than those based on the Pratt-Hayford model. Maximum smoothing (25 %) is thereby

achieved for spatial scales between 100 km and 400 km. The models also suggest that small scale topographic loads (smaller than 60 km for Airy-Heiskanen and 70 km for Pratt-Hayford) are no longer compensated. This agrees well with the geophysical fact that small-scale loads are supported by the strength of the lithosphere, see e.g. Watts (2001) and Torge (2003).

Acknowledgements

The authors appreciate the helpful comments by Dr. M.K. Kaban, the anonymous second referee and the editor of this issue.

References

Claessens, S., A synthetic Earth model. Analysis, implementation, validation and application (Delft University press, 2003).

Engels, J., Grafarend, E.W., and Sorcik, P. (1995), The gravitational field of topographic-isostatic masses and the hypothesis of mass condensation - Part I and II, Schriftreihe der Institute des Fachbereichs Vermessungswesen, Tech. rep. 1995.1, Department of Geodesy, Stuttgart.

Gruber, T. (2000), Hochauflösende Schwerefeldbestimmung aus Kombination von terrestrischen Messungen und Satellitendaten über Kugelfunktionen, Geoforschungszentrum Potsdam, Scientific Technical Report STR00/16.

Heiskanen, W.A. (1950), On the isostatic structure of the Earth's crust, Publ. of the Isostatic Institute of the IAG 24.

Heiskanen, W.A., and Moritz, H., Physical Geodesy (Freman and Company, San Francisco 1967).

Heck, B., and Wild, F., Topographic reductions in satellite gravity gradiometry based on a generalized condensation model, In A Window on the Future of Geodesy (ed. Sansô. F.) (Springer, Berlin Heidelberg New York 2005) pp. 294–299.

Kaban, M., Schwintzer, P., and Tikhotsky, A. (1999), A global isostatic gravity model of the Earth, Geophys. J. Int. 136, 519–536.

Kaban, M., Schwintzer, P., and Reigber, C. (2004), A new isostatic model of the lithosphere and gravity field, J. Geod. 78, 368–385.

Kuhn, M. (2003), Geoid determination with density hypotheses from isostatic models and geological information, J. Geod. 77, 50–65, DOI: 10.1007/s00190-002-0297-y.

Moritz, H., The Figure of the Earth (Wichmann, Karlsruhe 1990).

Mladek, F. (2006), Hydrostatische Isostasie, Schriftreihe IAPG/FESG No. 24, Institut für astronomische und physikalische Geodäsie, München.

Nakiboglu, S. M. (1982), Hydrostatic theory of the Earth and its mechanical implications, Physics of the Earth and Planetary Inter. 28, 302–311.

Rummel, R., Sünkel, H., Tscherning, C.C., and Rapp, R.H. (1988), Comparison of global topographic/isostatic models to the earth's observed gravity field, Dept. of Geodetic Science and Surveying, Ohio State University, Report No. 388.

Schubert, G., Turcotte, D.L., and Olson, P., Mantle Convection in the Earth and Planets (Cambrige University Press 2001).

Torge, W., Geodäsie (deGruyter Verlag, Berlin 2003).

Tsoulis, D. (1999), Spherical harmonic computations with topographic/isostatic coefficients, Schriftreihe des Institut für astronomische u. physikalische Geodäsie der TU München, Nr. 3.

Tsoulis, D. (2001), A comparison between the Airy/Heiskanen and the Pratt/Hayford isostatic models for the computation of potential harmonic coefficients, J. Geod. 74, 637–643, DOI: 10.1007/s001900000124.

Tsoulis, D. (2004), Spherical harmonic analysis of the CRUST 2.0 global crustal model, J. Geod. 78, 7–11, DOI:10.1007/s00190-003-0360-3.

Turcotte, D.L., and Schubert, G., Geodynamics (Wiley, New York 1982).

Watts, A. B., Isostasy and flexure of the lithosphere (Cambridge University Press 2001).

Wild-Pfeiffer, F. (2007), Auswirkungen topographisch-isostatischer Massen auf die Satellitengradiometrie, Deutsche Geodätische Kommission, Reihe C, Nr. 604, Verlag der Bayerischen Akademie der Wissenschaften, München.

Wild, F., and Heck, B. (2005), A comparison of different isostatic models applied to satellite gravity gradiometry, In Gravity, Geoid and Space Missions (eds. Jekeli. C., Bastos. L., Fernandes. J.) (Springer, Berlin Heidelberg New York 2005) pp. 230-235.

Wolf, D. (1984), Isostatic compensation and continental lithospheric thickness, J. Geophys. 54, 232–235.

Wolf, D. (1993), The changing role of the lithosphere in models of glacial isostasy, Global Planet. Change 8, 95–106.

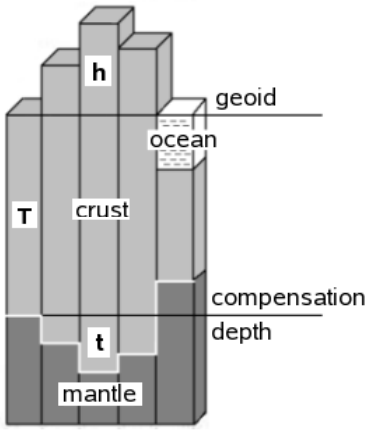

Figure 1: Airy-Heiskanen model, with topography of height h, compensation depth T and root thickness t.

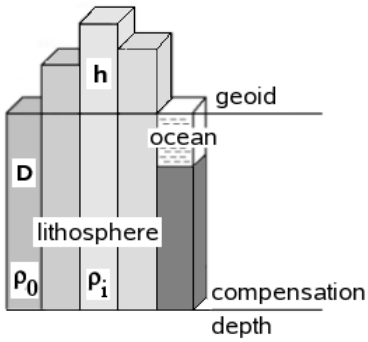

Figure 2: Pratt-Hayford model, with topography of height h, compensation depth D, average density of the lithosphere ρ_0 and variable density ρ_i.

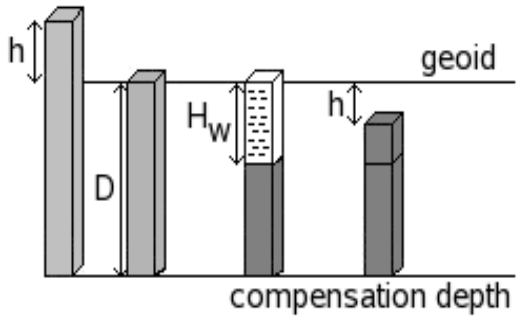

Figure 3: "Equivalent-rock" topography, with topography of height h, compensation depth D and water depth H_W.

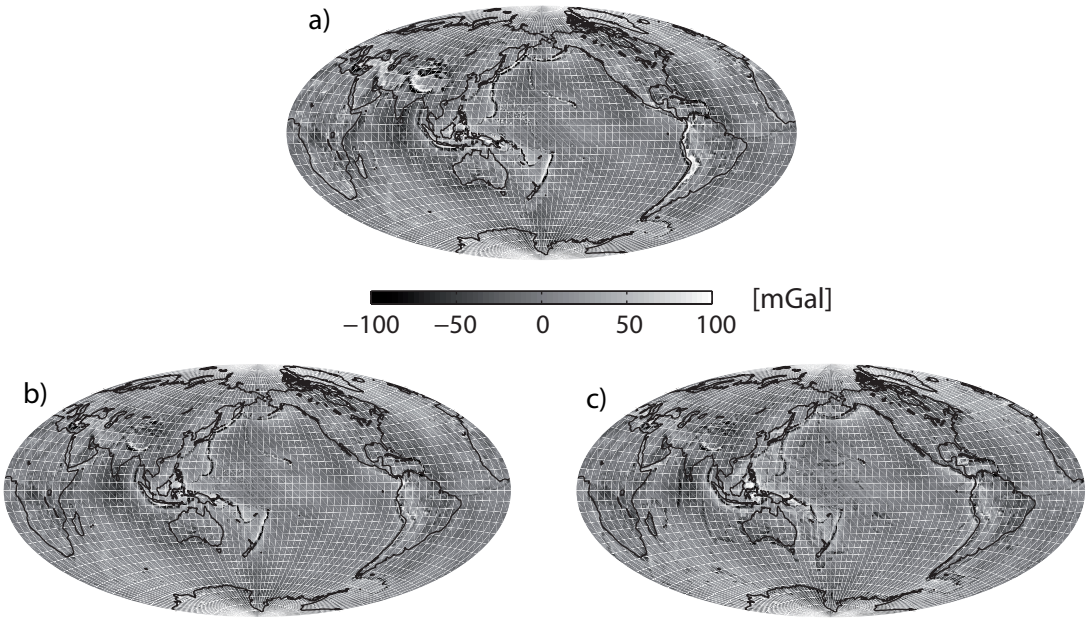

Figure 4: Maps of a) free air anomaly, b) Airy-Heiskanen isostatic anomaly and c) Pratt-Hayford isostatic anomaly.

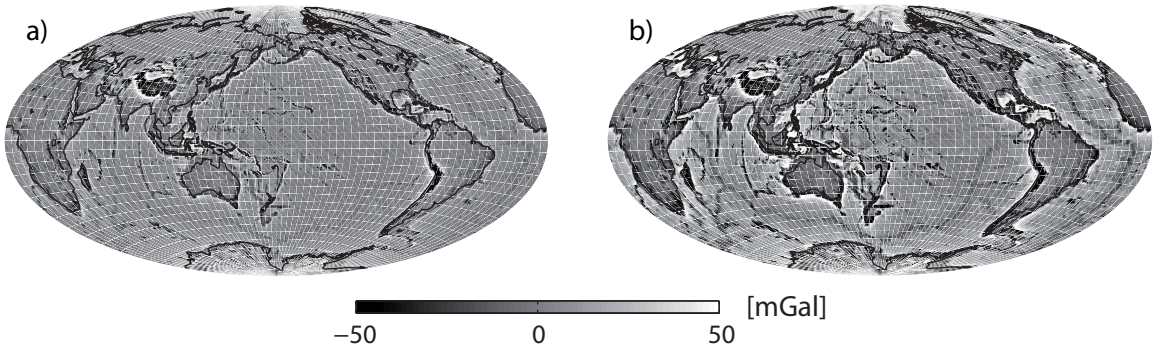

Figure 5: Maps of a) Airy-Heiskanen isostatic anomaly minus free air anomaly and b) Pratt-Hayford isostatic anomaly minus free air anomaly.

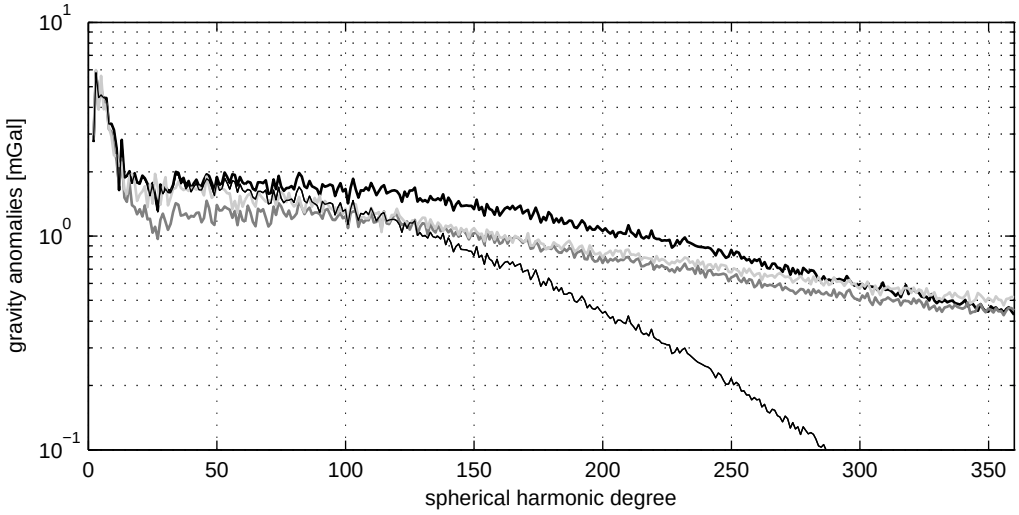

Figure 6: Degree RMS of free air anomaly (black, thick line), smoothed free air anomaly (black, thin line), isostatic anomaly of type Airy-Heiskanen (dark grey) and Pratt-Hayford (light grey).

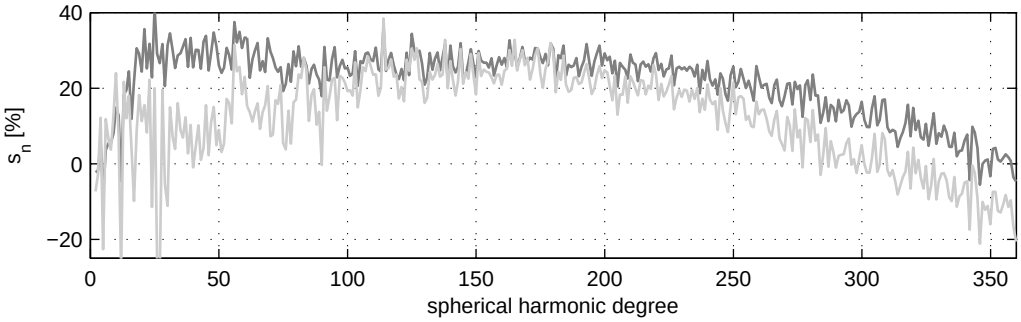

Figure 7: Smoothing percentage per spherical harmonic degree of isostatic relative to free air anomalies using the Airy-Heiskanen (dark grey) and the Pratt-Hayford model (light grey).

Table 1: Range of the values, mean and RMS value of free air, Airy-Heiskanen and Pratt-Hayford gravity anomalies for selected regions.

Geographical region	Δg^{FAR}	Δg^{Airy}	Δg^{Pratt}
Alps: $\theta = [40^\circ \quad 50^\circ]$; $\lambda = [0^\circ \quad 20^\circ]$			
min/max [mGal]	-107/102	-126/82	-133/92
mean [mGal]	15	12	9
RMS [mGal]	27	24	29
Andes: $\theta = [85^\circ \quad 125^\circ]$; $\lambda = [275^\circ \quad 295^\circ]$			
min/max [mGal]	-193/304	-125/180	-184/162
mean [mGal]	15	11	10
RMS [mGal]	52	31	32
Himalayas: $\theta = [50^\circ \quad 70^\circ]$; $\lambda = [70^\circ \quad 110^\circ]$			
min/max [mGal]	-230/339	-182/343	-188/327
mean [mGal]	-6	-16	-20
RMS [mGal]	54	34	33
Mariana T.: $\theta = [60^\circ \quad 80^\circ]$; $\lambda = [135^\circ \quad 155^\circ]$			
min/max [mGal]	-300/292	-243/202	-137/130
mean [mGal]	7	8	14
RMS [mGal]	47	38	30
Puerto-Rico-T.: $\theta = [60^\circ \quad 80^\circ]$; $\lambda = [290^\circ \quad 310^\circ]$			
min/max [mGal]	-330/182	-277/104	-221/62
mean [mGal]	-27	-24	-16
RMS [mGal]	42	34	34
Atacama T.: $\theta = [100^\circ \quad 130^\circ]$; $\lambda = [280^\circ \quad 290^\circ]$			
min/max [mGal]	-193/277	-111/183	-142/162
mean [mGal]	10	11	16
RMS [mGal]	61	35	33